Hygroscopicity frequency distributions of secondary organic aerosols

S. R. Suda,[1] M. D. Petters,[1] A. Matsunaga,[2] R. C. Sullivan,[3] P. J. Ziemann,[2] and S. M. Kreidenweis[3]

Received 1 September 2011; revised 7 December 2011; accepted 14 December 2011; published 22 February 2012.

[1] Secondary organic compounds are an important component of ambient aerosol and potentially lower the supersaturation that is required for individual particles to serve as cloud condensation nuclei (CCN). Secondary organic aerosol (SOA) formed from the oxidation of a single precursor can be composed of many different compounds and their overall CCN efficiency has been reported for many different SOA systems. An aerosol's CCN efficiency can be described by a single hygroscopicity parameter, κ. However, this κ comprises an unknown distribution of underlying κ-values resulting from each individual compound in the SOA mixture. Here we report on a new technique for characterizing this distribution of κ. Precursor hydrocarbons were oxidized in an environmental chamber to form SOA, which was collected on filters and extracted using ethyl acetate. Extracts were then fractionated by reversed-phase high-performance liquid chromatography using gradient elution with acetonitrile and water. The eluate was atomized, the solvent was removed by evaporation, and the residual aerosol particles were analyzed as a function of retention time using scanning flow CCN analysis. Kappa-values generally decreased with component retention time, consistent with expected decreasing polarity. Averaged SOA κ-values reconstructed by integrating over the chromatogram agreed well with values measured for SOA sampled directly from the environmental chamber, suggesting that κ for SOA represents the volume-weighted average of the constituent compounds' κ-values. We anticipate that our measured hygroscopicity distributions will serve as validation points for mechanistic models that seek to predict the generation and evolution of organic aerosol composition and properties in the atmosphere.

Citation: Suda, S. R., M. D. Petters, A. Matsunaga, R. C. Sullivan, P. J. Ziemann, and S. M. Kreidenweis (2012), Hygroscopicity frequency distributions of secondary organic aerosols, *J. Geophys. Res.*, *117*, D04207, doi:10.1029/2011JD016823.

1. Introduction

[2] Secondary organic aerosol (SOA) formed from the gas-phase oxidation of volatile organic compounds (VOCs) changes the distribution of particles that serve as cloud condensation nuclei (CCN) at prescribed supersaturations [e.g., *Gunthe et al.*, 2009]. This leads to indirect modification of cloud and precipitation spectra, which feeds back on the Earth's radiation budget and hydrological cycle [e.g., *Andreae and Rosenfeld*, 2008]. To better characterize these effects, a large number of studies have measured the CCN efficiency of compounds identified in ambient organic aerosol (e.g., carboxylic acids and carbohydrates, see auxiliary material from *Petters et al.* [2009a] for a list of compounds) as well as SOA generated inside environmental chambers using a diverse assortment of VOCs and oxidants [e.g., *VanReken et al.*, 2005; *Prenni et al.*, 2007; *King et al.*, 2007; *Duplissy et al.*, 2008; *Engelhart et al.*, 2008; *Asa-Awuku et al.*, 2010]. One way to parameterize the results from these studies is to report the hygroscopicity parameter κ [*Petters and Kreidenweis*, 2007], which allows comparisons of CCN efficiency for different compounds or mixtures. Remarkably, the κ-values for SOA derived from the oxidation of isoprene, monoterpenes, and toluene, compounds representative of most of the major VOC classes, fall within the narrow envelope $\kappa = 0.1 \pm 0.04$. Organic aerosol mass concentration [*King et al.*, 2009], VOC:NO_x ratio [*King et al.*, 2010], the concentration of water vapor, and the identities of OH scavengers present during an ozonolysis reaction [*Poulain et al.*, 2010] seem to exert only minor influences on the observed κ-values.

[1]Department of Marine Earth and Atmospheric Sciences, North Carolina State University, Raleigh, North Carolina, USA.
[2]Air Pollution Research Center, University of California, Riverside, California, USA.
[3]Department of Atmospheric Science, Colorado State University, Fort Collins, Colorado, USA.

0148-0227/12/2011JD016823

[3] These results are surprising, since SOA formed from these reactions is composed of many compounds with a large variety of structures [*Kroll and Seinfeld*, 2008]. For example, the α-pinene ozonolysis reaction yields many hundreds of products with different H:C and O:C ratios [*Heaton et al.*, 2009] and combinations of functional groups such as carbonyl, hydroxyl, carboxyl, hydroperoxy, and ester [*Yu et al.*, 1999; *Docherty et al.*, 2005]. Based on current understanding of atmospheric VOC reaction mechanisms [e.g., *Atkinson and Arey*, 2003], absorptive gas-particle partitioning [*Pankow*, 1994; *Odum et al.*, 1996; *Donahue et al.*, 2006], and the effect of molecular properties on CCN efficiency [*Petters et al.*, 2009a], the CCN experiments that systematically varied reaction conditions [*Poulain et al.*, 2010; *King et al.*, 2010] and mass concentration [*King et al.*, 2009] should have probed a wide range of molecular compositions, and thus a range of κ-values. One would expect this range to even be larger in the atmosphere; however, κ is also near 0.1 for the organic fraction of ambient aerosol [*Shantz et al.*, 2008; *Wang et al.*, 2008; *Gunthe et al.*, 2009; *Shinozuka et al.*, 2009; *Dusek et al.*, 2010; *Cerully et al.*, 2011]. This begs the question, "Why does composition appear to have such a minor effect on the κ-values of these complex SOA mixtures"?

[4] One way to address this question is to measure the κ-values of the components of organic mixtures obtained by physical (e.g., distillation) or chemical (e.g., solvent extraction) methods of fractionation. For example, *Asa-Awuku et al.* [2010] extracted the water-soluble fraction of several SOAs using the method of *Sullivan and Weber* [2006] and subjected them to CCN analysis. Based on their results, they proposed that the aerosols can be conceptualized as an effective two-component mixture with invariant values of κ = 0.3 for the water-soluble fraction and κ = 0 for the water-insoluble fraction, and that the remarkably small variations in SOA κ-values are attributable to small variations in the relative fraction of water-soluble compounds.

[5] Here we report data acquired using a new method we have developed that involves separating complex SOA mixtures using reversed-phase high-performance liquid chromatography coupled with high-resolution scanning flow CCN analysis to determine κ-values of mixture components. We apply this method to filter extracts of SOA formed from many different VOC-oxidant combinations to survey κ frequency distributions resulting from a broad range of chemical reactions. Theory predicts that the volume-weighted average of the measured κ frequency distribution should reproduce the κ-value measured for the SOA sampled from the environmental chamber directly into the CCN analyzer (and thus without extraction), and we show that this is indeed the case. Using the combined results from all experiments we examine the relationship between retention time, which is expected to increase with decreasing component polarity, and measured κ-value. For selected systems we demonstrate the correspondence of the κ frequency distribution with expectations based on differences in reaction products. Our results should aid in the development of structure-activity relationships that can predict an organic compound's κ-value based on its chemical structure. Such relationships would provide a means for predicting aerosol hygroscopicity using the aerosol composition computed from atmospheric chemical transport models.

2. Methods

2.1. Köhler Theory

[6] Köhler Theory relates the saturation ratio over a water droplet and the droplet's diameter via

$$S = a_w \exp\left(\frac{4\sigma_{s/a}M_w}{RT\rho_w D}\right) \quad (1)$$

where S is the saturation ratio, a_w is the water activity, $\sigma_{s/a}$ is the surface tension of the solution-air interface, ρ_w is the density of water, M_w is the molecular mass of water, R is the universal gas constant, T is the temperature, and D is the droplet diameter.

[7] We parameterize the water activity using the functional form proposed by *Petters and Kreidenweis* [2007]

$$S = \frac{D^3 - D_d^3}{D^3 - D_d^3(1-\kappa)} \exp\left(\frac{4\sigma_{s/a}M_w}{RT\rho_w D}\right) \quad (2)$$

where D_d is the particle dry diameter and κ is the hygroscopicity parameter. The critical saturation ratio, S_c, is defined by the maximum of equation (2); κ can be estimated from experimentally determined S_c and D_d values by

$$\kappa = \frac{4A^3}{27D_d^3 \ln^2(S_c)},\ A = \frac{4\sigma_{s/a}M_w}{RT\rho_w} \quad (3)$$

[8] When computing κ from experimental data, T = 298 K and $\sigma_{s/a}$ = 0.072 J m^{-2} are assumed in order to yield a data set that is self-consistent among different studies.

[9] The Zdanovskii, Stokes, and Robinson (ZSR) assumption states that the total water content equals to the sum of the water contents of the individual components. For particles that are composed of multiple components and for which the ZSR assumption holds, the κ-value for a mixture of components is the sum of the volume-weighted component κ-values

$$\kappa = \sum_i \varepsilon_i \kappa_i \quad (4)$$

where ε_i is the volume fraction of component i, and κ_i is that component's κ-value.

2.2. SOA Generation

[10] The following chemicals with purities and suppliers were used: 1-octene (98%), 1-decene (94%), cis-cyclooctene (95%), 1,3-cyclohexadiene (97%), 1,5-cyclooctadiene (99+%), 1,3,5,7-cyclooctatetraene (98%), 2,3-dimethyl-2-butene (98%), *n*-decane (99+%), *n*-pentadecane (99+%), cyclooctane (99+%), cyclodecane (95%), *m*-xylene (99+%), 2-propanol (99.5%) (Sigma-Aldrich); dioctyl sebacate (≥97%), β-caryophyllene (99%) (Fluka); cyclohexane (99.9%) (Fisher Scientific); 1,2-dimethyl cyclohexene (97%) (ChemSampCo); 3-methyl furan (98%) (Acros Organic); ocimene (99+%) (IFF Inc.); cyclohexene (99%) (Chemical Samples Co.); chlorine (99.5%) (Matheson Tri-Gas); and nitric oxide (99.5%) (Airgas). Methyl nitrite [*Taylor et al.*, 1980] and dinitrogen

Table 1. Summary of Oxidation Reactions Performed[a]

Experiment Number	Label: VOC + Oxidant	VOC (ppmv)	Oxidant or Precursors	ppmv of Oxidant or Precursors	$V_{chamber}$ (m^3)	$\kappa_{chamber}$	κ_{HPLC}	Concentration ($\mu g\ m^{-3}$)
1	1-decene + O_3, RH 20%[b]	1.2	O_3	7.0	1.7	0.04	0.02	~1300
2	ocimene + NO_3	0.7	N_2O_5	2.0	1.7	0.04	0.04	~4500
3	1,3-cyclohexadiene + NO_3	0.3	N_2O_5	0.6	1.7	0.03	0.05	~110
4	1,5-cyclooctadiene + NO_3 A	0.3	N_2O_5	0.6	1.7	0.07	0.05	~750
5	1,3,5,7-cyclooctatetraene + NO_3	0.3	N_2O_5	1.2	1.7	0.03	0.05	~2000
6	1,5-cyclooctadiene + NO_3 B	0.3	N_2O_5	0.6	1.7	0.07	0.06	~750
7	3-methyl furan + OH with NO_x[c]	10.0	CH_3ONO/NO	10/10	5.9	0.07	0.06	N/A
8	1-decene + O_3, RH 82%	1.2	O_3	7.0	1.7	0.09	0.08	~700
9	*n*-pentadecane + Cl (9 July A)	0.5	Cl_2	2.0	5.9	0.06	0.08	~3600
10	*n*-pentadecane + Cl (9 July B)	0.5	Cl_2	2.0	5.9	0.06	0.08	~3600
11	*n*-decane + Cl, 1st irr.	0.5	Cl_2	8.0	5.9	0.08	0.09	~850
12	*n*-pentadecane + Cl (13 July)	0.1	Cl_2	0.2	5.9	0.09	0.09	~450
13	*n*-pentadecane + Cl (16 July B)	0.5	Cl_2	0.5	5.9	0.05	0.09	~1000
14	cyclodecane + OH with NO_x	0.3	CH_3ONO/NO	6.5/5.5	5.9	0.11	0.10	~360
15	*n*-pentadecane + Cl (16 July A)	0.5	Cl_2	0.5	5.9	0.05	0.10	~1500
16	1-octene + O_3 + 2-propanol	0.4	O_3	7.0	1.7	0.11	0.12	~270
17	*n*-pentadecane + Cl (8 July B)	0.1	Cl_2	2.0	5.9	0.15	0.15	~540
18	*n*-pentadecane + Cl (8 July A)	0.1	Cl_2	2.0	5.9	0.15	0.15	~540
19	*m*-xylene + OH with NO_x[c]	4.0	CH_3ONO/NO	4.0/4.0	5.9	0.07	0.16	N/A
20	1,2-dimethyl cyclohexene + O_3	0.5	O_3	7.0	1.7	0.15	0.17	~300
21	*n*-decane + Cl, 2nd irr.	0.5	Cl_2	8.0	5.9	0.16	0.17	~800
22	cyclooctene + O_3	1.1	O_3	7.0	1.7	0.12	0.20	~1600
23	cyclohexene + O_3	1.0	O_3	7.0	1.7	0.17	0.22	~1200
24	cyclooctane + OH w/o NO_x	5.6	TME/O_3[d]	7.0/1.4	1.7	0.13	0.22	~45

[a]The number in column 1 is an identifier for experiments shown in Figure 7. $V_{chamber}$ denotes the volume of the chamber used for the experiment.
[b]All ozonolyis reactions included 1000:1 (ppm:ppm) excess of cyclohexane to scavenge OH radicals formed during the reaction, and β-caryophyllene as a precursor to seed aerosol.
[c]Experiments 7 and 19 used dioctyl sebecate (DOS) seed aerosol.
[d]TME, trimethyl ethylene (2,3-dimethyl-2-butene); experiment 24 used β-caryophyllene as a precursor to seed aerosol.

pentoxide [*Atkinson et al.*, 1984] were synthesized and stored under vacuum in liquid nitrogen. Ozone (2% ozone in O_2) was generated using a Welsbach T-408 ozone generator. Purchased chemicals were used without further purification.

[11] SOA was generated from reactions performed with a suite of VOCs and oxidants that were selected to result in a wide variety of chemical compositions and κ-values. The VOC-oxidant reactions studied are summarized in Table 1, and include the reactions of simple linear and cyclic alkenes with ozone (O_3) in the presence of a hydroxyl (OH) radical scavenger; linear and cyclic alkenes with nitrate (NO_3) radicals; aromatics with OH radicals in the presence of NO_x; and alkanes with chlorine (Cl) atoms or OH radicals in the absence of NO_x.

[12] SOA was generated inside a 1.7 or 5.9 m^3 FEP Teflon environmental chamber operated at room temperature (~298 K) and pressure [*Matsunaga and Ziemann*, 2010]. The chamber was flushed and filled with dry (RH < 1%), hydrocarbon-free (<5 ppbv) air from an Aadco clean air generator. The VOC was added to the chamber by flushing clean air through a 500 mL glass bulb that contained a measured volume or mass of the liquid or solid VOC. The bulb was heated slightly with a heat gun when necessary to evaporate the VOC and guarantee that all constituents entered the chamber. The oxidant was either added directly to the chamber or generated in situ. O_3 was flushed into the chamber from a glass bulb. NO_3 radicals, Cl atoms, and OH radicals were generated in the chamber: NO_3 radicals by thermal dissociation of N_2O_5, Cl atoms by photolysis of Cl_2, and OH radicals in the presence of NO_x by photolysis of a mixture of methyl nitrite (CH_3ONO) and NO (added to suppress O_3 and NO_3 radical formation) [*Atkinson et al.*, 1981] or in the absence of NO_x by reaction of tetramethylethylene (TME) with O_3, which produces OH radicals with a yield close to 1 [*Atkinson*, 1997]. Desired chamber concentrations of N_2O_5, Cl_2, methyl nitrite, or NO were obtained by adding a measured pressure of gas to a calibrated glass bulb on a glass vacuum rack and then flushing into the chamber with clean air. Photolysis was carried out using blacklights (λ_{max} = 360 nm) that covered two walls of the 5.9 m^3 chamber. For reactions of alkenes with NO_3 radicals or O_3, VOC:oxidant ratios were chosen such that all C = C double bonds were reacted. For reactions with Cl atoms or OH radicals, which occur by H-atom abstraction, the average number of abstractions was controlled by adjusting VOC:radical precursor ratios and/or the duration and intensity of blacklight irradiation. For reactions with Cl atoms, the number of abstractions is given approximately by the molar ratio, Cl:VOC (Table 1). For reactions with OH radicals, the number of abstractions depends on the duration and intensity of light exposure.

[13] In order to obtain particle size distributions suitable for CCN analysis it was necessary in most experiments to add to the chamber, in addition to the major VOC, a trace amount of a highly reactive VOC whose very low volatility reaction products rapidly nucleated to form high concentrations of small seed particles onto which the SOA condensed. The seed particles increased the SOA particle number concentration and decreased the mode diameter, bringing the mode diameter of the size distribution into the range required for CCN analysis. Specifically, β-caryophyllene was added for reactions with O_3 and some of the reactions with OH radicals. In two cases, dioctyl sebecate (DOS) seed particles generated with an evaporation-condensation source [*Matsunaga et al.*, 2009] were instead added directly to the chamber (see Table 1). The amounts of major VOC

and β-caryophyllene or DOS added were chosen to achieve <1% mass of seed relative to SOA. The volume fraction of seed material varied between particle sizes because the condensation rate is proportional to particle surface area and the size distribution evolved by coagulation. Nonetheless, the expected average contribution of the seed material to the aerosol volume and thus its κ-value is <1% and this value is smaller than the resolution of the κ measurement.

[14] Reactions were initiated by adding the oxidant to the chamber or by turning on the blacklights to initiate oxidant formation via photolysis. Particles rapidly formed via homogeneous nucleation (except when DOS seed was present), and the size distribution evolved as reaction products condensed and particles coagulated. A few minutes after initiating the reaction, the sampling line was connected to a port in the chamber wall and the particle size distribution and CCN activation properties were measured online. CCN measurements were completed in ~1 h and then particle samples were collected on Millipore filters (0.45 μm pore size, Fluoropore FHLP, 47 mm) at a flow rate of 15 L min^{-1} [*Matsunaga and Ziemann*, 2010]. Based on reaction conditions and kinetics the oxidant is expected to have been completely depleted at the time of sampling. Filter sample collection took ~1 h and then filters were stored at low temperature, where further oxidation was unlikely.

2.3. Measurement of CCN Efficiency of SOA Sampled Directly From the Chamber

[15] The CCN setup was identical to that used by *Petters et al.* [2009b]. In brief, particles were sampled directly from the chamber through copper tubing and passed through two diffusion dryers and a ^{210}Po neutralizer before entering a differential mobility analyzer (DMA) (TSI model 3080, sheath-to-sample flow ratio 9:1.5) to select a specified mobility diameter. The dryers are included to ensure that water is removed from aerosol formed in the presence of water vapor. The flow was then split between a condensation particle counter (CPC, TSI 3010) and a CCN counter (CCNC, Droplet Measurement Technologies, sheath-to-sample flow ratio 10:1) [*Roberts and Nenes*, 2005] to measure total particle concentration and CCN concentration at constant water supersaturation. Particle size and CCN distributions were obtained by stepping through several dry diameters. The ratio of CCN to total particle concentration defines the CCN response curve from which the activation diameter was determined via an inversion procedure that accounts for multiply charged particles [*Petters et al.*, 2007, 2009b]. The relationship between the temperature gradient and supersaturation in the CCNC was calibrated using dry ammonium sulfate particles [*Rose et al.*, 2008]. The temperature gradient and particle diameter were set by the CCNC and DMA, respectively. Activation diameters from the ammonium sulfate particles were used to compute the supersaturation in the instrument using the relationship between water activity and composition from the Extended Aerosol Inorganic Model (E-AIM) [*Clegg et al.*, 1998; *Wexler and Clegg*, 2002].

[16] For a few experiments, size distributions were measured using a scanning mobility particle sizer (SMPS) that measured directly from the chamber (sheath-to-aerosol flow ratio ~5:1, size range varied from 50–600 to 100–800 nm). For all other experiments, size distributions were obtained from the CCN setup (sheath-to-aerosol flow ratio 9:1.5, size range 25–320 nm). SMPS mass concentrations were estimated by integration over the size distribution and assuming an aerosol density of 1 g cm^{-3}. Mass concentrations from the CCN setup were determined by fitting a lognormal function to the size distribution. This procedure was necessary because the descending branch of the size distribution often exceeded the upper size range of the measurement. Because these large particles were not captured well by this method, the reported mass concentrations are only an approximate estimate. Mass concentrations increased while the aerosol was forming and decreased due to continually occurring wall losses. The average mass concentrations over the duration of chamber CCN data collection periods are reported in Table 1.

2.4. Measurement of CCN Efficiency of HPLC-Fractionated SOA

2.4.1. Generation of HPLC-Fractionated SOA Particles

[17] The method used to generate HPLC-fractionated SOA particles for CCN analysis is similar to one we used previously for mass spectrometric analysis [*Ziemann*, 2005; *Matsunaga and Ziemann*, 2009]. Filter samples of SOA from the chamber experiments were extracted in ethyl acetate, which we have shown previously to efficiently extract all SOA compounds [*Docherty et al.*, 2005; *Matsunaga and Ziemann*, 2009]. Filters were pre-cleaned by immersing them twice in 10 mL of ethyl acetate at room temperature for >10 min and drying in a stream of N_2. After sampling, filters were extracted immediately or stored at −20°C for up to 2 days. Filters were extracted twice in flasks containing 4 mL ethyl acetate at room temperature for >10 min following 30 s of agitation, and the extracts were combined. Extracts were analytically transferred into a vial with a conical insert, dried in a stream of N_2, and dissolved in acetonitrile to achieve 50–600 μg in a 10 μl injection. The mass of the dry extract was compared to the increase in filter mass during sampling; the extraction was >98% efficient. The extract was then fractionated using an Agilent 1100 series HPLC outfitted with a 250 × 4.6 mm Zorbax 5 μm Eclipse XDB-C18 column operating at room temperature with a guard column [*Matsunaga and Ziemann*, 2009]. The method employed gradient elution with a constant flow rate of 1 mL min^{-1} using water and acetonitrile, with the acetonitrile concentration increasing linearly from 5% for 10 min to 100% over a 50 min interval. Experiments using organic acid standards indicated that negligible material eluted between acid peaks, and extracts taken from blank pre-cleaned filters produced negligible mass. We therefore believe that the results were not biased by solvent impurities. With this method, compounds elute from the column in the order of decreasing polarity. Eluate from the column was passed directly to a Collison atomizer jet. The atomizer was continuously flushed by the HPLC solvents, and no residue accumulated or was atomized. Aerosol from the atomizer was subsequently passed through a pair of diffusion dryers, one containing activated charcoal and the other silica gel, to remove evaporated organic solvents and water, respectively. The residual aerosol particles were charge-neutralized using a ^{210}Po neutralizer and size classified using a DMA (TSI 3081, sheath:sample flow ratio varying from 10:0.7 to 10:1.7). The size-classified particle flow was split between a CPC

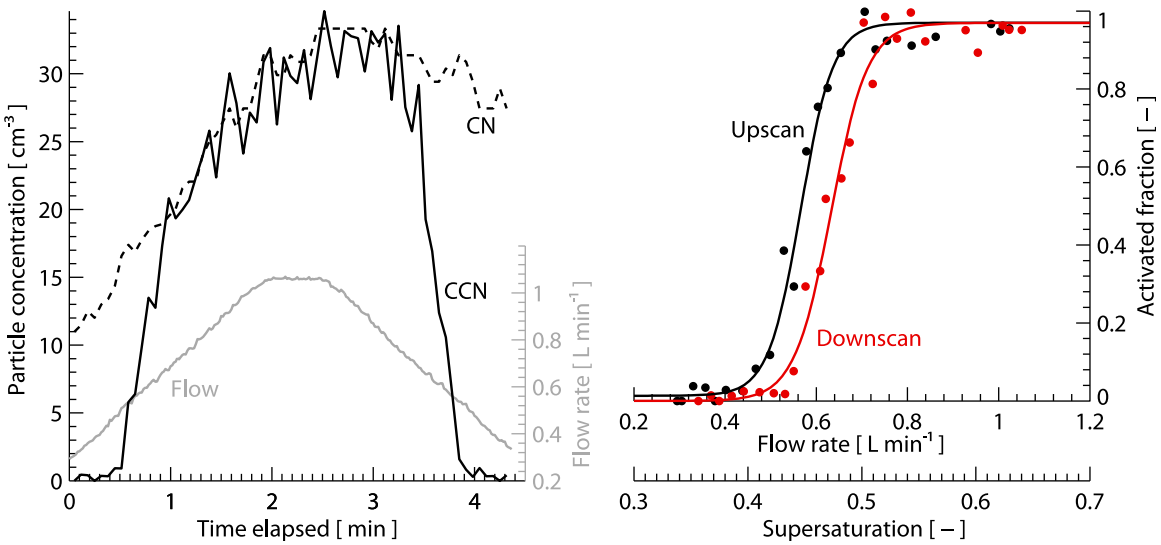

Figure 1. (left) Example duty cycle illustrating the flow rate (gray line), CCN (solid black line) and CN (dashed line) time series. (right) Inferred CCN activation curve for the upscan (black circles) and downscan (red circles). Each circle represents a 4 s average. Lines represent a fit to the data from which the flow at 50% activation is inferred.

and a DMT CCNC instrument operating in scanning flow mode [*Moore and Nenes*, 2009]. The particle concentration measured by the CPC indicated the quantity of material eluting from the HPLC column. The concentration time series is referred to hereafter as the chromatogram.

2.4.2. Scanning Flow Cycle

[18] The scanning flow CCN measurement method imposes a linear flow profile at a constant linear column temperature gradient (ΔT = 7°C) to control the varying supersaturation in the CCNC column. When coupled with monodisperse aerosol, the method is equivalent to traditional supersaturation scans but operates at much higher time resolution. Total flow was controlled by continuously varying the direct current voltage supplied to an externally installed blower (flow rate 0.2 to 1.2 L min^{-1}). Each 2 min flow scan was separated by a 30 s interval of constant flow rate to allow the system to flush. The duty cycle, shown in Figure 1, lasted 5 min, consisting of an upscan during which flow was increased and downscan during which flow was decreased. Raw data were recorded at 1 Hz and each upscan and downscan was processed using the procedure described below.

2.4.3. Time Series Processing

[19] Due to the continuous variation in flow rate, the ratio of CPC and CCNC residence times was not constant; therefore, the raw CPC and CCNC time series were misaligned. The delay between the two detectors was measured by placing a HEPA filter upstream and recording the flush time for each instrument. Repeating this procedure for different flow rates resulted in an empirical relationship between the delay and flow rate that is well described by $\Delta t = A/Q + B$, where Δt is the delay, Q is the total flow rate in the CCNC, and A and B are constants fitted to the data. To align the data, the CPC time series was shifted by Δt according to the instantaneous flow rate. The CPC and CCNC data reported in Figure 1 show an example after the alignment procedure and demonstrate excellent agreement, as is seen when all condensation nuclei (CN) activated as CCN at high flow rates.

[20] After alignment, the 1 Hz data were averaged into 4 s bins to reduce noise stemming from low counting statistics. The CCN response curve shown in Figure 1 (right) shows the ratio between the CCNC and CPC time series as a function of flow rate. A sigmoid activation curve [*Sullivan et al.*, 2009] was fitted to the response curve for each upscan and downscan:

$$y = \frac{A_{\min} - A_{\max}}{1 + \exp([Q - Q_{50}]/dx)} + A_{\max} \quad (5)$$

where y is the fitted activated fraction, $A_{\min}$ is the lower limit of activation, $A_{\max}$ is the upper limit of activation, Q is the flow, Q_{50} is the flow at 50% activation, and dx is the rate of change in activated fraction with respect to the increasing flow rate.

2.4.4. Flow-to-Supersaturation Calibration

[21] The relationship between Q_{50} and supersaturation was determined by calibration with atomized ammonium sulfate particles [*Rose et al.*, 2008]. The supersaturation at activation was modeled for each dry diameter using E-AIM [*Clegg et al.*, 1998; *Wexler and Clegg*, 2002] and correlated with the experimentally determined Q_{50} value for those diameters. Figure 2 shows an example of the relationship between modeled supersaturation and experimental Q_{50} for 10 dry diameters. A nearly linear calibration curve of the form $s_c = CQ_{50}^E$ was applied to fit the data, where C and E are the fitted constants. Typically, a calibration curve of this type was obtained once per day. Calibrated supersaturation for the upscan and downscan are slightly different, which *Moore and Nenes* [2009] attributed to wall thermal effects and droplet inertial effects. For particles of unknown composition, the experimentally determined Q_{50} from size-selected aerosol was used with the calibration to assign the

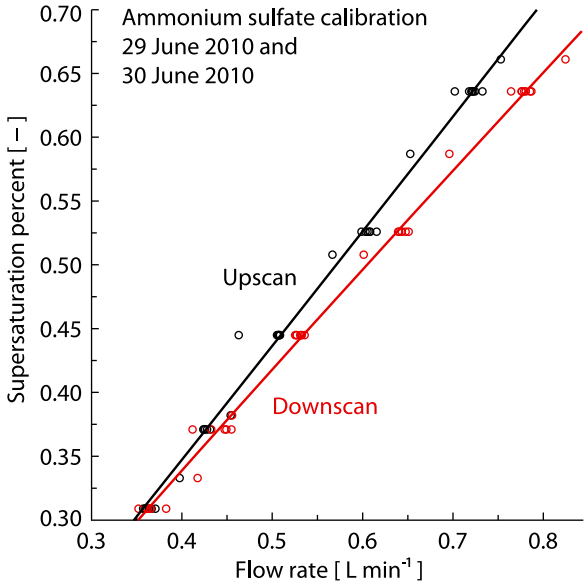

Figure 2. Relationship between CCNC flow rate at 50% activated fraction and calculated supersaturation percent for size selected ammonium sulfate particles.

critical supersaturation. The resulting dry diameter and critical supersaturation were then used to compute the κ-value using equation (3). With this method, κ-values could be determined approximately every 2.5 min.

2.4.5. Envelope of Resolvable κ-Values

[22] The dynamic range of the supersaturation differs slightly for each scan due to small changes in the minimum and maximum flow rates, but is usually between 0.3% and 0.7%, as shown in Figure 2. Combined with the selected dry diameter, this corresponds to an envelope of κ-values that can be resolved for any particular flow scan. Because κ-values are expected to decrease with increasing retention time due to elution of less polar products, we programmed a stepwise increase of dry diameter with each scan, thereby moving the envelope to smaller κ-values. Typically 12 diameters were measured between 50 and 200 nm, corresponding to a κ-envelope of $0.004 < \kappa < 1.22$. An activation curve was fitted to each scan. Any κ-values falling above the envelope were discarded; low particle number concentration resulted in poor fits of these activation curves to the data. An average of one out of 24 κ-values was discarded per HPLC experiment. Kappa-values falling below the envelope were adjusted to the envelope, providing an upper estimate of the κ-value for these compounds.

2.4.6. Reconstructing the κ-Value of SOA From Component κ-Values

[23] One useful test of the validity of our approach for measuring component κ-values is to reconstruct the κ-value of the SOA using equation (4), for comparison with the value measured by directly sampling SOA from the chamber into the CCN counter. However, this reconstruction requires knowledge of the volume fraction of each fractionated component in the sample. To determine these volume fractions a number of assumptions were made, which are discussed below.

[24] The first assumption is that for a given line pressure and solvent mixture, the atomizer produces a constant number concentration of droplets. In our experiments, the number concentration of droplets is not constant during elution, but increases with retention time because of the gradual increase in the acetonitrile:water ratio. This lowers the surface tension of the solvent mixture, leading to increased droplet breakup. This is demonstrated in Figure 3, which shows the size distribution for pentadecane + Cl SOA. This experiment was chosen to characterize the atomizer output because a continuum of products eluted from the HPLC column without gaps. The number concentration obtained from integration over the size distribution increased from $\sim 6 \times 10^4$ cm^{-3} at 2–13 min to $\sim 16 \times 10^4$ cm^{-3} at 35–46 min retention time. The atomizer would have produced a constant number concentration if it had not been affected by the increasing acetonitrile fraction, which caused an estimated threefold increase in number concentration in the 60 min scan. We corrected for this increase by scaling the measured number concentration at time $t + \Delta t$ using a linear gradient, making it equal to number concentrations measured at time t. This number scaling was performed for all experiments, providing a quantity N_{scaled} for each retention time.

[25] The second assumption is that the shape of the droplet size distribution is constant, implying that the dried aerosol distribution shifts to larger diameters with increasing droplet

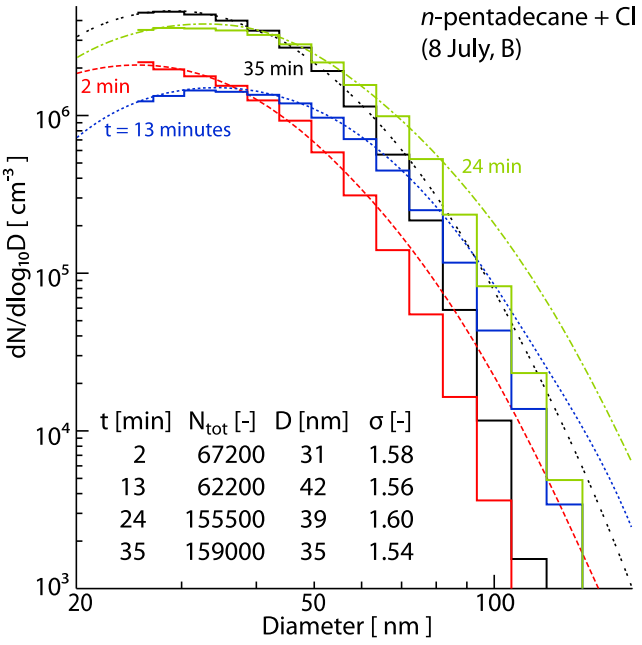

Figure 3. Size distribution of particles from the HPLC CCN measurement system for SOA from an *n*-pentadecane + Cl experiment, as measured by the online CCN measurement setup. Times reported are the start times for the 11 min scans. The stepped lines show the measured size distribution over the scan, and the dotted lines show a fit to the data. The integrated total count over the fit, N_{tot}, the mode diameter, D, and the standard deviation, σ, are noted in a table below the distributions.

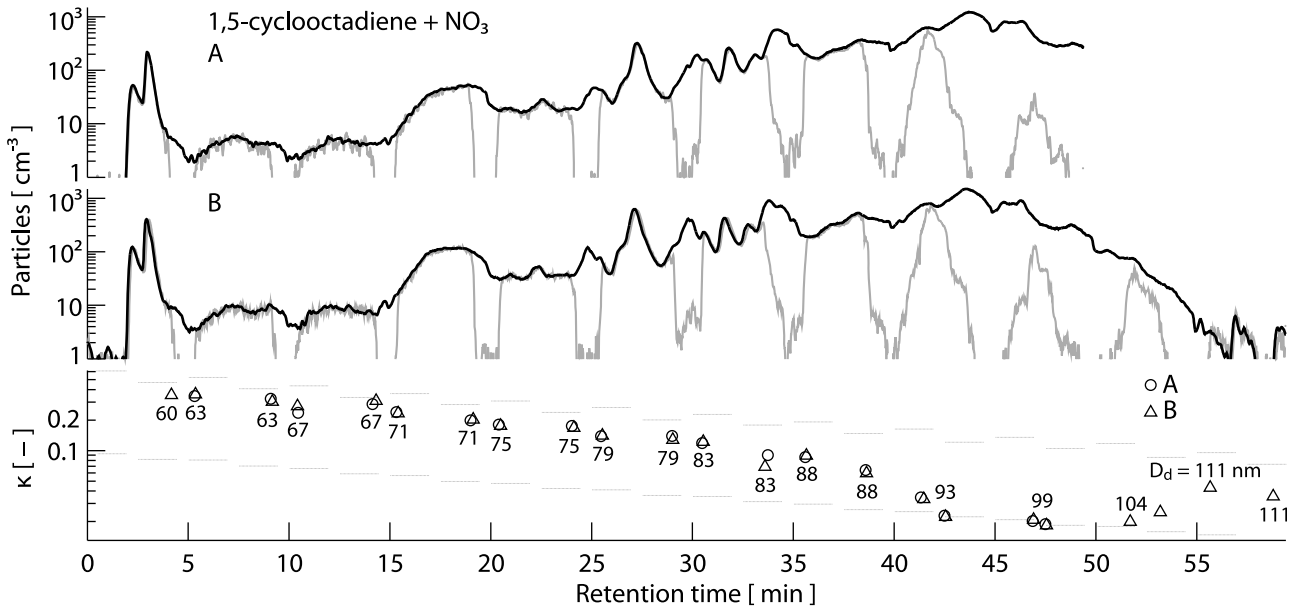

Figure 4. CN (black lines) and CCN (gray lines) concentrations versus HPLC retention time, for the SOA from 1,5-cyclooctadiene + NO_3 (top) A and (middle) B using the same filter extract. (bottom) The κ-values (symbols) and envelope of measurable κ-values (gray lines) versus HPLC retention time for 1,5-cyclooctadiene + NO_3 A (circles) and B (triangles). The selected dry diameter is indicated below the symbols. Scan A was terminated prematurely due to erroneous software settings.

solute concentration. The number density of particles at diameter $D + \Delta D$ is lower than at diameter D provided that the selected diameter is larger than that of the mode diameter. Mass concentrations of solute in the filter sample were generally similar between experiments, and particles with $50 < D_d < 200$ nm were used for all HPLC experiments. Given the observed mode diameters in Figure 3, we assume that our diameters were sampled along the descending branch of the size distribution. A curve of the form $N = FD_d^{-G}$ approximates the atomized particle size at the upper tail of a lognormal distribution, where N is the number concentration, D_d is dry diameter, and F and G are constants. We compute the effective number concentration $N_{D,ref}$ we would expect at a selected reference diameter using

$$N_{D,ref} = N_{scaled}\left(\frac{D_{ref}}{D_d}\right)^{-G} \quad (6)$$

where $G = 2 \pm 2$ captures the full range of slopes. $G = 0$ corresponds to a uniform size distribution and $G = 4$ captures the observed upper end of the slope produced by the atomizer.

[26] The third assumption is that the mode diameter of the dried aerosol size distribution is smaller than the diameters we used in our experiments, which allows us to use equation (6) as an estimate of the number concentration at the reference diameter. The quantity $N_{D,ref}$ serves as proxy for the amount of solute in the eluate. This is because higher solute concentrations correspond to a shift toward larger mode diameters [*Liu and Lee*, 1975], thereby raising the number concentration of particles larger than the mode diameter. The increase in number concentration with higher solute concentration is nearly linear if the fixed reference diameter is much larger than the mode diameter [*Suda*, 2011]. Thus, the total volume and corresponding volume fractions are obtained by numerical integration of the particle concentration over time, i.e., the chromatogram. Formally the volume fraction of the ith scan is given by:

$$\varepsilon_i = \frac{\int_{scan} N_{D,ref}\, dt}{\int_{chromatogram} N_{D,ref}\, dt}. \quad (7)$$

[27] An example chromatogram including the raw time series and the processed κ-values is shown in Figure 4 for SOA generated from the reaction of 1,5-cyclooctadiene + NO_3 radicals. We note that in each chromatogram there is an initial peak occurring at $t \sim 3$ min. This peak contains all compounds which are not retained by the C18 column. The peak was generally narrow and the compounds were highly hygroscopic which prevented us from capturing it consistently in our setup. We therefore excluded the first peak from the analysis of all the chromatograms, and the resulting shift in reconstructed κ-values is discussed in section 2.4.7.

[28] The individual κ_i and ε_i were aggregated into histograms shown in Figure 5. These were constructed in log-κ space using geometrically spaced κ bins to achieve equidistant histogram bars. Bar heights were determined by summing the ε_i associated with κ_i falling within the bin bounds. The choice of bin width has no effect on the averaged SOA κ-value, which was computed from the κ_i and ε_i for each scan cycle using the mixing rule described by equation (4). This volume-weighted average value is indicated on each histogram.

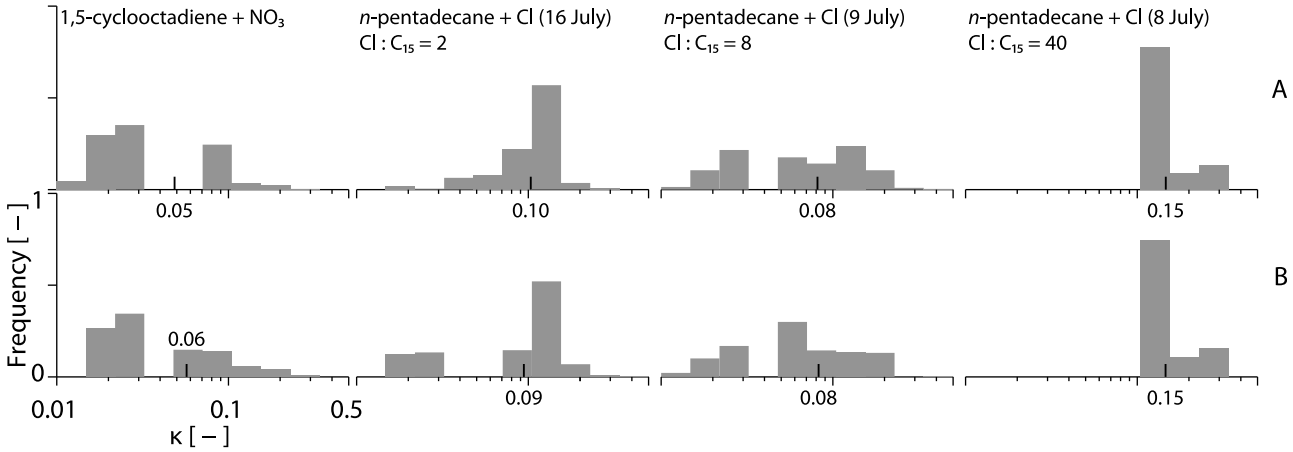

Figure 5. Kappa frequency distributions of pairs of repeated HPLC experiments using the same filter extract. (top) Experiment A and (bottom) experiment B. The oxidant:precursor ratio for each *n*-pentadecane + Cl chamber experiment is indicated on the plot as $Cl:C_{15}$. The averaged κ-value, as reconstructed by equation (4), is indicated with a small vertical line and printed value.

2.4.7. Uncertainties and Reproducibility of Individual κ Measurements

[29] The main uncertainties of this procedure stem from the increase of particle number concentration with retention time due to droplet breakup and the slope of the descending branch of the size distribution. Repeating the analysis with no scaling parameter results in a ~6% shift in the reconstructed κ-value. Changing the slope parameter G by ± 2 leads to an average difference in reconstructed κ-value of $\pm 9\%$ depending on the distribution of products. Including the chromatogram's initial peak resulted in a ~20% increase in the reconstructed κ-value. Faster scans could be used to better capture this peak. We tested the reproducibility of the method by splitting the filter extract into two samples that were analyzed separately. Figure 4 shows the HPLC eluate and κ-values for the repeated injection of a 1,5-cyclooctadiene + NO_3 filter extract, and Figure 5 shows κ distributions of several repeat injections. The chromatograms and resultant reconstructed κ-values generally compare well ($R^2 = 0.98$, $n = 4$).

3. Results and Discussion

[30] The chromatogram shown in Figure 4 for SOA generated from the reaction of 1,5-cyclooctadiene + NO_3 radicals contains some peaks as narrow as ~60 to 90 s, typical of single compounds, but is dominated by broader peaks indicative of a highly complex mixture. Kappa-values are reported as a function of retention time and graphed at the estimated time that Q_{50} was observed. The values are spaced unevenly over time because activation may occur at any point during the upscan or downscan. One noteworthy observation from the chromatogram is that constituent compounds making up the SOA samples elute from the HPLC with a continuum of κ-values that decreased almost monotonically with retention time for a single scan. Figure 6 pools the relationship between κ-values and retention time for all systems measured using the HPLC-CCN method, showing that there is ~1 order of magnitude spread in the κ-values of compounds eluting from the HPLC at any given retention time. The spread demonstrates that κ is not a unique function of retention time. However, the κ-value of the HPLC eluate generally decreased with retention time, as expected, since in reversed-phase chromatography compounds elute in order of decreasing polarity and less polar compounds are expected to be less hygroscopic.

[31] Figure 7 summarizes the hygroscopicity distributions for several systems, grouped by the reconstructed SOA κ-value obtained via the volume-weighted integration of the chromatogram. The data show that SOAs with similar reconstructed κ-values can have substantially different underlying κ distributions, which reflect differences in the hygroscopicities of the constituent compounds. For example, whereas the reconstructed κ-values for SOA formed from the reactions of 1,3,5,7-cyclooctatetraene + NO_3 and 3-methyl furan + OH in the presence of NO_x (Figure 7 (top), third and fourth columns) were similar, at $\kappa = 0.05$ and $\kappa = 0.06$, respectively, the first SOA had a broad distribution of values that ranged from about 0.02 to 0.20 while the second SOA had a narrow distribution centered at 0.06. Similarly, SOA formed from the reactions of cyclohexene + O_3 and cyclooctane + OH without NO_x had the same reconstructed κ-value of 0.22, but whereas the first SOA had a narrow distribution of values centered at 0.20 the second SOA had a much broader distribution (Figure 7 (bottom), third and fourth columns). Thus, while the hygroscopicity of individual products may vary substantially, the volume-weighted average is less sensitive to these variations, as shown by the tendency for κ-values of SOA formed from different VOC reactions to be similar (e.g., from α-pinene ozonolysis [*Prenni et al.*, 2007] and photooxidation of isoprene [*King et al.*, 2007]).

[32] In an attempt to substantiate this conclusion, in Figure 8 we compare the reconstructed SOA κ-values (κ_{HPLC}) to the SOA κ-values measured by online analysis of SOA sampled directly from the chamber (κ_{online}). The values correlate reasonably well, with a trend in the data given by $\kappa_{HPLC} = 1.19\ \kappa_{online}$ ($R^2 = 0.66$, $n = 24$). Although there appears to be a slight high bias in the HPLC-derived values, we consider the agreement to be good, especially given the

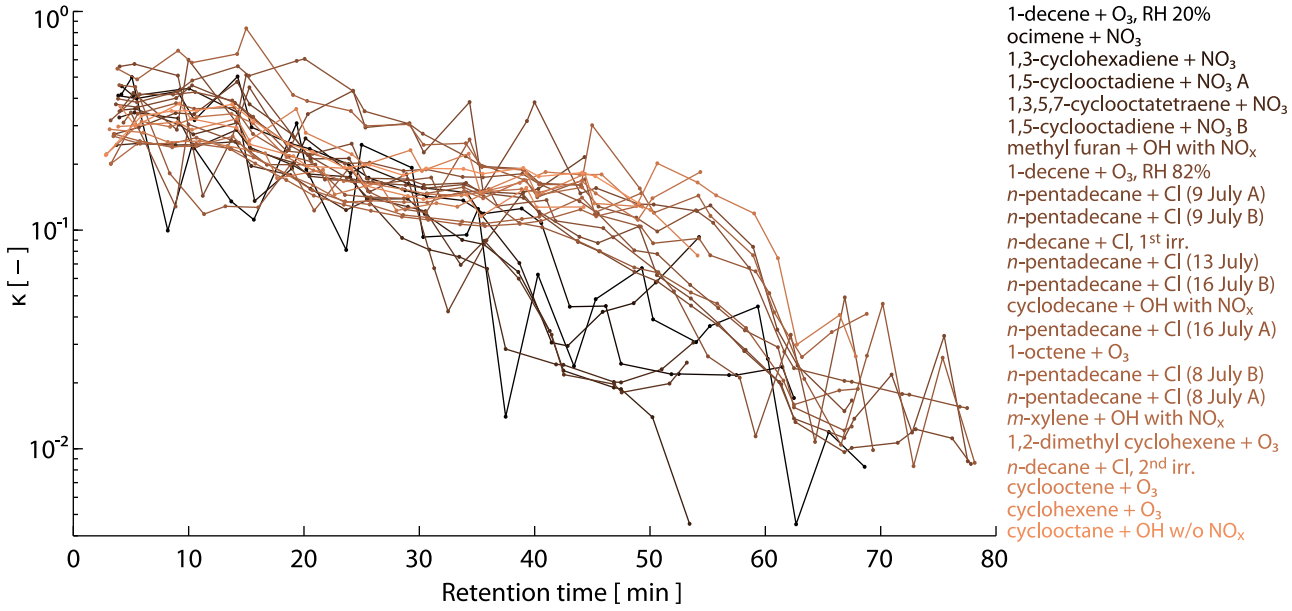

Figure 6. The HPLC eluate hygroscopicities for all experiments as a function of their retention time.

assumptions that were necessary to obtain the volume fractions of eluting compounds in the mixture. The high bias in the HPLC-derived values occurs despite the removal of the first diameter in each scan, whose κ-value was typically very high. Although the HPLC-CCN measurements had a higher time resolution than the online CCN measurements, sharp peaks in the chromatogram sometimes eluted before a flow scan was completed. This forced the measured κ-values into bins of similar retention time. Specifically, if CCN activation occurs just before a peak in the chromatogram, the κ-value attributed to the peak will reflect the κ-value at activation, measured close to but not concurrently with the κ-value at the time of the peak. The scanning flow CCN duty cycle should be shortened in future applications of this technique to avoid this issue.

[33] For an ideal system, the ZSR mixing rule predicts a 1:1 correspondence between κ_{HPLC} and κ_{online}. Aside from experimental uncertainty involved in characterizing the volume fraction and κ values of the eluate, additional factors can lead to a degradation of the 1:1 relationship. The CCNC instrument requires heating to form a supersaturation, and may remove volatile compounds from the aerosol and change the measured CCN properties [*Asa-Awuku et al.*, 2009]. For the HPLC-CCN experiments ΔT = 7°C was selected while

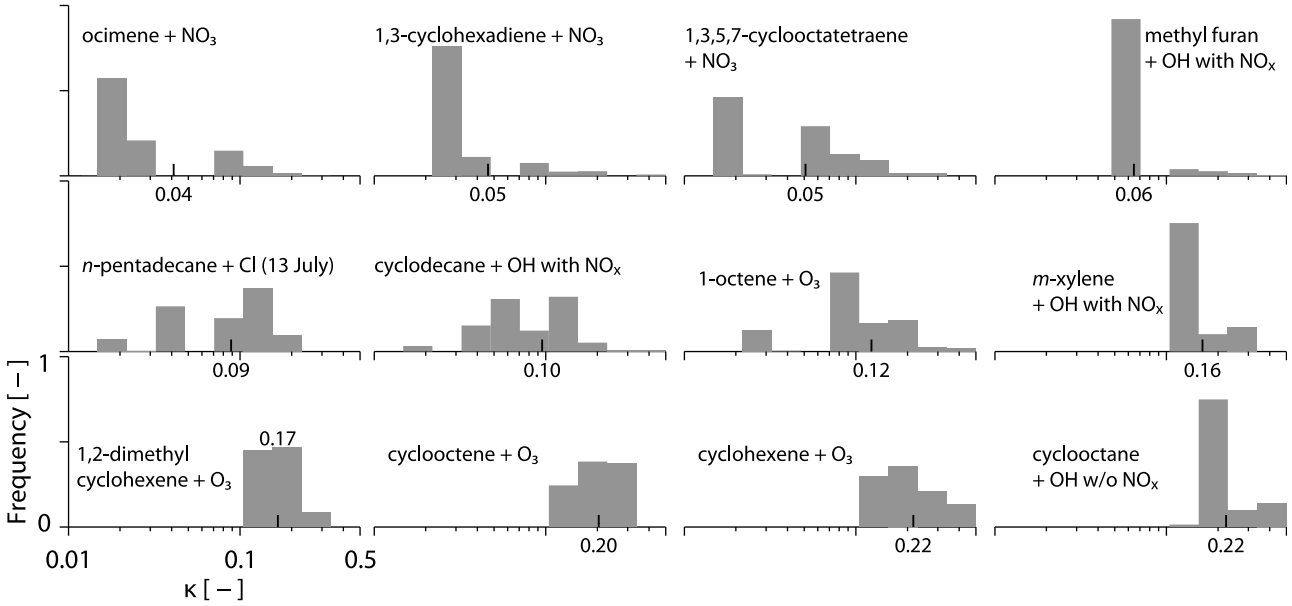

Figure 7. Kappa frequency distributions of selected SOA systems. The averaged κ-value, as reconstructed by equation (4), is indicated with a small vertical line and printed value.

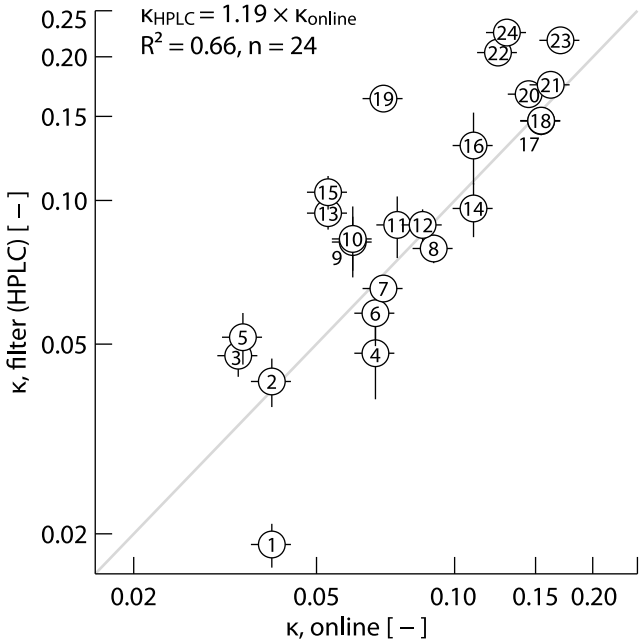

Figure 8. Scatterplot of reconstructed HPLC eluate κ-values versus κ-values measured for SOA sampled directly from the chamber, with the 1:1 line in gray. Numbers on the graph correspond to the experiment number given in Table 1. Horizontal bars indicate the sensitivity of the HPLC κ-value to the choice of exponent G in the size correction. Vertical bars indicate the uncertainty in the online κ-value determined from the reproducibility of the calibration.

for the online experiments ΔT varied between 3 and 16°C. The diffusion dryers may have removed semivolatile compounds. The charcoal denuders in the HPLC-CCN setup necessarily remove the organic HPLC solvent, but volatile aerosol components are also lost and the losses may differ between the two setups. If chemical reactions occurred during filter collection (either further oxidation or heterogeneous reactions) κ_{HPLC} and κ_{online} should also deviate from the 1:1 line.

[34] The preceding factors should all be classified as potential measurement artifacts. Deviation from the 1:1 line, however, may also occur due to non-ZSR mixing. Nonlinear mixing can arise from solute-solute interactions or because surface tension affects particles differently when present in the internal mixture compared to when studied in isolation.

[35] We believe that the SOA κ distributions shown here have the potential to provide quantitative links between SOA hygroscopicity and the chemical reaction mechanisms involved in SOA formation. Because the wealth of data presented here is beyond the scope of complete analysis at this time, we focus on two particular systems to demonstrate this potential.

[36] Two experiments were performed with 1-decene + O_3 in which the reaction conditions were identical except for the amount of H_2O vapor present in the chamber. Figure 9 (left) shows the κ frequency distributions resulting from these experiments, and Figure 10 shows a simplified diagram of the reactions and products. Briefly, the chemistry of the reaction [*Tobias and Ziemann*, 2001] can be summarized as follows: the reaction between 1-decene and O_3 results in the formation of formaldehyde and nonanal, C_1 and C_9 stabilized Criegee intermediates (SCI), and some minor C_1 and C_9 carboxylic acids. Subsequently, the C_1-SCI reacts further to form formic acid and other small products, but reactions of C_1-SCI do not form aerosol. The C_9-SCI reacts with H_2O, formaldehyde, nonanal, and formic acid to produce α-hydroxy-nonyl-hydroperoxide, C_{10} and C_{18} secondary ozonides (SOZ), and α-alcyloxy-nonyl-hydroperoxide, respectively. The C_{10} SOZ is volatile and not expected to be in the condensed phase. The relative amounts of the other products depends on the availability of H_2O molecules. At low relative humidity, the dominant product is the C_{18} SOZ, and as RH is increased the product distribution shifts toward α-hydroxy-nonyl-hydroperoxide. The C_{18} SOZ is expected to have a lower κ-value than the α-hydroxy-nonyl-hydroperoxide due to its large molar volume, lower O:C ratio (κ scales inversely with molar volume [*Petters et al.*, 2009a] and correlates with the O:C ratio [*Jimenez et al.*, 2009; *Chang et al.*, 2010; *Duplissy et al.*, 2011]), and reduced tendency for hydrogen bonding. The observed κ distributions are consistent with this chemical mechanism, revealing a cluster of low-κ products when the reaction RH is low (20%) and an increased fraction of high-κ products when the reaction proceeds at high RH (82%). However, even at high RH some low-κ compounds remain visible in the spectra. These may be due to the formation of peroxyhemiacetals from the reaction of the α-hydroxy-nonyl-hydroperoxide with gas phase aldehydes occurring on the surface of the particle [*Tobias and Ziemann*, 2001]. The peroxyhemiacetal is expected to have a lower κ-value because of its larger molar volume and lower O:C ratio, more nearly similar to the C_{18} SOZ.

[37] Another set of experiments was performed by reacting *n*-decane and *n*-pentadecane with Cl atoms. Chlorine atoms

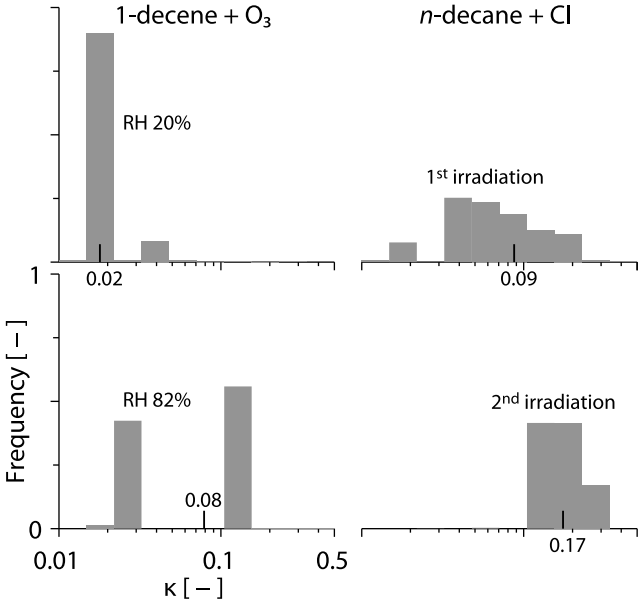

Figure 9. Kappa frequency distributions of SOA from the 1-decene + O_3 and *n*-decane + Cl chamber experiments. The averaged κ-value, as reconstructed by equation (4), is indicated with a small vertical line and printed value.

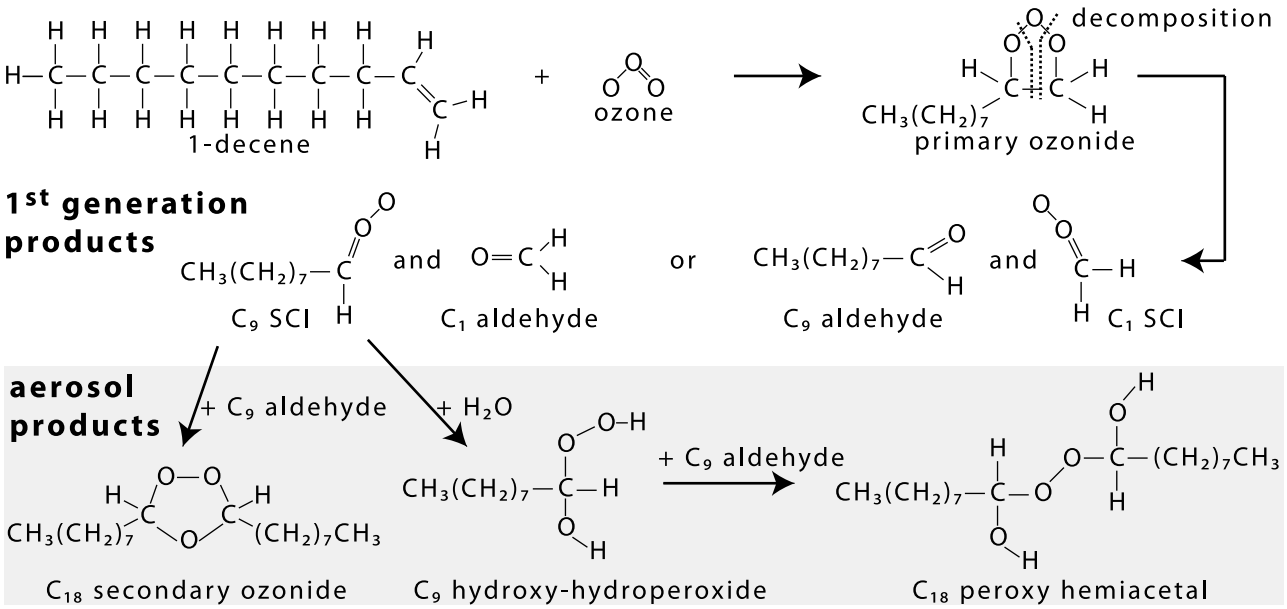

Figure 10. Schematic of the mechanism of reaction of 1-decene + O_3. SCI denotes stabilized Criegee Intermediate.

initiate reaction by abstracting H atoms from the carbon chain, similarly to H atom abstraction by OH radicals [*Atkinson*, 1997; *Atkinson and Arey*, 2003]. The degree of oxidation can be controlled by the amount of Cl_2 added to the chamber and the duration of blacklight exposure. In our experiment the *n*-decane + Cl_2 mixture was irradiated twice, with a separate filter sample collected after each irradiation. *n*-Pentadecane experiments were performed at various Cl: VOC ratios. Because the aerosol collected after the second irradiation was more oxidized, we expect its κ-value to be higher. The histograms in Figure 9 (right) and Figure 5 confirm this prediction, showing that the κ frequency distribution is generally shifted toward higher κ-values when more oxidant was present. The less hygroscopic products ($\kappa < 0.10$) become more hygroscopic while the products at the higher end of the distribution ($\kappa > 0.10$) appear unchanged. One possible explanation is a SOA formation mechanism similar to one suggested by *Robinson et al.* [2007], in which the SOA becomes more highly oxidized over time due to coupling between gas-phase oxidation and gas-particle partitioning. In this scenario, semi-volatile products present in the gas phase undergo further reactions to form more highly oxidized products that condense due to their lower volatility. The semi-volatile products lost from the gas phase by reaction are subsequently replaced by evaporation of less oxidized compounds from the particles, maintaining gas-particle partitioning equilibrium. The net result is that particles become more oxidized as the less oxidized products are replaced by more oxidized products. In our examples, the low-κ products are expected to be more volatile than the high-κ products, and are thus replaced by these high-κ products in the particles as oxidation proceeds. However, κ does not always increase with decreasing volatility. Volatility decreases with molecule size and with functionalization [*Joback and Reid*, 1987; *Goldstein and Galbally*, 2007]. Reactions may lengthen molecules by oligomerization or shorten them by fragmentation [*Cappa et al.*, 2011; *Kroll et al.*, 2009]. Kappa-values decrease with molar volume [*Petters et al.*, 2009a], but are expected to increase with functionalization. These conflicting dependencies on molecule size and functionalization complicate the relationship between κ and volatility.

[38] Another application of the HPLC-CCN method is to measure κ-values for compounds that are formed in chamber reactions but are otherwise inaccessible for CCN studies because they are not commercially available. This can be done, for example, by performing chamber experiments with VOC-oxidant systems that yield a small number of SOA products that can be separated by HPLC. The relationship between hygroscopicity and polarity shown in Figure 6 suggests that a compound's κ-value can be predicted by analysis of molecular functional groups. Further tests can be designed to probe the relationship between functional groups and κ-value by coupling the HPLC output to a chemical composition measurement such as with a thermal desorption particle beam mass spectrometer (as we have done previously [*Ziemann*, 2005; *Matsunaga and Ziemann*, 2009]) while simultaneously measuring the κ-value.

[39] Our hygroscopicity frequency distributions extend the results of *Asa-Awuku et al.* [2010], adding finer κ resolution. In their study, the CCN properties were determined from filter extracts using pure water. The water-soluble SOA was found to have an average κ-value of $\sim$0.3, and the remaining sample was assumed to have $\kappa = 0$. Applying the mixing rule, the overall κ-value was thus found to be the volume fraction of water-soluble organic carbon multiplied by 0.3. In this study we extracted SOA using ethyl acetate, a moderately polar solvent, and fractionated the extract by HPLC using acetonitrile-water mixtures. Because of the large range in component polarities indicated by the chromatograms, we expect that filter extraction with water, a highly polar solvent, would be a less efficient than with ethyl acetate. The bulk value of $\kappa = 0.3$ for water-soluble SOA found by *Asa-Awuku et al.* [2010] is likely the average of a broader range of constituent κ-values. Although our data sometimes shows the

presence of compounds with $\kappa < 0.004$, i.e., compounds that do not activate at the diameter and supersaturation combination achieved in our setup, their fraction is generally small. As is shown in Figure 6, many of the κ-values measured here were higher than 0.3. We therefore believe that a binary distinction between water-soluble and water-insoluble ($\kappa = 0$) organic compounds does not capture the full complexity of the hygroscopicity distribution of SOA components. Many of the hygroscopicity distributions, however, are either bimodal, do not contain products with $\kappa < 0.05$, or both (cf., Figure 7), and thus describing organic aerosol mixtures as the combination of a hygroscopic and non-hygroscopic fraction might be suitably accurate for many applications.

[40] The highest observed κ-values of individual compounds likely represents an upper limit that can be achieved for aged organic aerosol in the atmosphere. For selected individual compounds [*Petters et al.*, 2009a] as well as chemical aging experiments on mixtures [*Massoli et al.*, 2010; *Lambe et al.*, 2011] the observed upper limit is ~0.3. To reach these high κ-values one would expect that the molar volume is small and that the compounds are water soluble [*Petters et al.*, 2009a; *Cappa et al.*, 2011]. Based on this we would expect that hygroscopicity distributions of highly aged SOA will have a narrow dispersion around its average value, and that the physicochemical properties of the aged compounds are similar. Our highest chamber SOA values were 0.22 and thus lower than those representing the hypothetical endpoint of aging. This may be due in part to the high mass loadings of our experiments, which will allow for partitioning of less polar compounds into the mixture. Furthermore, even though our experiments covered a broad range of oxidant: VOC ratios and thus a broad range of oxidation, our aerosol did not reach the hypothetical endpoint of oxidation. Atmospheric hygroscopicity distributions may therefore differ significantly from those presented here, and studying ambient hygroscopicity distributions or those of highly aged SOAs generated in the laboratory [*Massoli et al.*, 2010; *Lambe et al.*, 2011] may reveal additional valuable information about the evolution of organic aerosol composition and properties in the atmosphere.

4. Summary and Conclusions

[41] We present a new method, HPLC-CCN analysis, which couples high-performance liquid chromatography with scanning flow CCN analysis to characterize the distribution of the hygroscopicity parameter for polarity-separated constituents of complex SOA. The observed distributions reveal that the investigated SOA comprises a diverse array of products with hygroscopicities in the range $\sim 0 < \kappa < \sim 0.4$, with some product κ-values below the measurement envelope. Some SOA systems are composed of a few products with distinct κ-values while others exhibit a broad spectrum of component κ-values. For two selected systems we show that the distribution of SOA κ-values is consistent with current mechanistic understanding of SOA formation. For example, we demonstrate that our method resolves changes in the hygroscopicity distribution of SOA formed from the 1-decene + O_3 reaction – changes consistent with expected changes in the product distribution for reactions run at different relative humidities.

[42] Our results show that the distributions of constituent κ-values vary widely over a range of SOA systems. This is consistent with the range of chemical mechanisms and products that govern the formation of SOA from the different VOC and oxidant combinations. Most distributions are broad and consist of a continuum of κ-values rather than a pseudo-binary mixture of water-soluble and water-insoluble ($\kappa = 0$) compounds. However, the CCN activity of the chamber SOA is less varied because of the averaging effect of the mixture. We demonstrate that SOA κ-values can be reconstructed from those of the constituents resolved by the HPLC separation. For the 24 systems studied here, the reconstructed κ-values agreed well with the SOA κ-values measured by direct sampling and analysis of chamber SOA ($R^2 = 0.66$, $n = 24$). Because SOA comprises many compounds with a broad spectrum of κ-values, and because the κ of the SOA is a volume-weighted average of these values, it is reasonable that SOAs formed from the reactions of hundreds of VOCs with OH radicals, O_3, and NO_3 radicals have relatively smaller variability in their net κ-value despite the different sources and compositions.

[43] The HPLC method separates compounds according to the polarity of the molecules, with less polar products eluting at later times. As expected, we found that κ-values decreased with increasing retention time and thus with decreasing polarity. However, the retention time did not unambiguously determine the κ-value, showing ~1 order of magnitude spread for any given retention time. Nevertheless, the relationship between a compound's κ-value and its polarity suggests that a relationship may exist between a compound's κ-value and its functional group composition and carbon number, which determine a compound's polarity.

[44] The method described here might also be useful in future studies for constraining proposed chemical mechanisms of SOA formation. For simple systems with a few reaction products, the HPLC separation might yield individual product peaks for which κ can be determined. If reaction products cannot be identified but are predicted by modeling, and product κ-values can be computed, then the result will be a hygroscopicity distribution that can be directly compared to measurements. The resultant κ distributions are further useful in exploring mechanisms that relate changes in κ to chemical reactions such as chemical aging, as we demonstrated by contrasting different oxidation stages of SOA generated from the oxidation of *n*-decane and *n*-pentadecane. Future applications of this method could effectively combine modeling and chamber experiments to improve our understanding of the chemical mechanisms underlying the formation and evolution of organic aerosol composition and properties.

[45] **Acknowledgments.** This research was funded by the Office of Science (BER), U.S. Department of Energy, under DE-FG02-05ER63984. We thank Sukon Aimanant and Christen Strollo Gordon for their assistance with some of the experiments.

References

Andreae, M. O., and D. Rosenfeld (2008), Aerosol-cloud-precipitation interactions. Part 1. The nature and sources of cloud-active aerosols, *Earth Sci. Rev.*, *89*(1–2), 13–41, doi:10.1016/j.earscirev.2008.03.001.

Asa-Awuku, A., G. J. Engelhart, B. H. Lee, S. N. Pandis, A. Nenes, and S. N. Pandis (2009), Relating CCN activity, volatility, and droplet growth kinetics of β-caryophyllene secondary organic aerosol, *Atmos. Chem. Phys.*, *9*(3), 795–812, doi:10.5194/acp-9-795-2009.

Asa-Awuku, A., A. Nenes, S. Gao, R. C. Flagan, and J. H. Seinfeld (2010), Water-soluble SOA from Alkene ozonolysis: Composition and droplet activation kinetics inferences from analysis of CCN activity, *Atmos. Chem. Phys.*, *10*(4), 1585–1597, doi:10.5194/acp-10-1585-2010.

Atkinson, R. (1997), Gas-phase tropospheric chemistry of volatile organic compounds: 1. Alkanes and alkenes, *J. Phys. Chem. Ref. Data*, *26*(2), 215–290, doi:10.1063/1.556012.

Atkinson, R., and J. Arey (2003), Atmospheric degradation of volatile organic compounds, *Chem. Rev.*, *103*(12), 4605–4638, doi:10.1021/cr0206420.

Atkinson, R., W. P. L. Carter, A. M. Winer, and J. N. Pitts Jr. (1981), An experimental protocol for the determination of OH radical rate constants with organics using methyl nitrite photolysis as an OH radical source, *Air Pollut. Control Assoc.*, *31*, 1090–1092.

Atkinson, R., C. N. Plum, W. P. L. Carter, A. M. Winer, and J. N. Pitts (1984), Rate constants for the gas-phase reactions of nitrate radicals with a series of organics in air at 298 $\pm$ 1 K, *J. Phys. Chem.*, *88*(6), 1210–1215, doi:10.1021/j150650a039.

Cappa, C. D., D. L. Che, S. H. Kessler, J. H. Kroll, and K. R. Wilson (2011), Variations in organic aerosol optical and hygroscopic properties upon heterogeneous OH oxidation, *J. Geophys. Res.*, *116*, D15204, doi:10.1029/2011JD015918.

Cerully, K. M., et al. (2011), Aerosol hygroscopicity and CCN activation kinetics in a boreal forest environment during the 2007 EUCAARI campaign, *Atmos. Chem. Phys. Discuss.*, *11*(5), 15,029–15,074, doi:10.5194/acpd-11-15029-2011.

Chang, R. Y.-W., J. G. Slowik, N. C. Shantz, A. Vlasenko, J. Liggio, S. J. Sjostedt, W. R. Leaitch, and J. P. D. Abbatt (2010), The hygroscopicity parameter (κ) of ambient organic aerosol at a field site subject to biogenic and anthropogenic influences: Relationship to degree of aerosol oxidation, *Atmos. Chem. Phys.*, *10*(11), 5047–5064, doi:10.5194/acp-10-5047-2010.

Clegg, S. L., P. Brimblecombe, and A. S. Wexler (1998), Thermodynamic model of the system H^+–NH_4^+–SO_4^{2-}–NO_3^-–H_2O at Tropospheric Temperatures, *J. Phys. Chem. A*, *102*(12), 2137–2154, doi:10.1021/jp973042r.

Docherty, K. S., W. Wu, Y. B. Lim, and P. J. Ziemann (2005), Contributions of organic peroxides to secondary aerosol formed from reactions of monoterpenes with O_3, *Environ. Sci. Technol.*, *39*(11), 4049–4059, doi:10.1021/es050228s.

Donahue, N. M., A. L. Robinson, C. O. Stanier, and S. N. Pandis (2006), Coupled partitioning, dilution, and chemical aging of semivolatile organics, *Environ. Sci. Technol.*, *40*(8), 2635–2643, doi:10.1021/es052297c.

Duplissy, J., et al. (2008), Cloud forming potential of secondary organic aerosol under near atmospheric conditions, *Geophys. Res. Lett.*, *35*, L03818, doi:10.1029/2007GL031075.

Duplissy, J., et al. (2011), Relating hygroscopicity and composition of organic aerosol particulate matter, *Atmos. Chem. Phys.*, *11*(3), 1155–1165, doi:10.5194/acp-11-1155-2011.

Dusek, U., G. P. Frank, J. Curtius, F. Drewnick, J. Schneider, A. Kürten, D. Rose, M. O. Andreae, S. Borrmann, and U. Pöschl (2010), Enhanced organic mass fraction and decreased hygroscopicity of cloud condensation nuclei (CCN) during new particle formation events, *Geophys. Res. Lett.*, *37*, L03804, doi:10.1029/2009GL040930.

Engelhart, G. J., A. Asa-Awuku, A. Nenes, and S. N. Pandis (2008), CCN activity and droplet growth kinetics of fresh and aged monoterpene secondary organic aerosol, *Atmos. Chem. Phys.*, *8*(14), 3937–3949, doi:10.5194/acp-8-3937-2008.

Goldstein, A. H., and I. E. Galbally (2007), Known and unexplored organic constituents in the Earth's atmosphere, *Environ. Sci. Technol.*, *41*(5), 1514–1521, doi:10.1021/es072476p.

Gunthe, S. S., et al. (2009), Cloud condensation nuclei in pristine tropical rainforest air of Amazonia: Size-resolved measurements and modeling of atmospheric aerosol composition and CCN activity, *Atmos. Chem. Phys.*, *9*(19), 7551–7575, doi:10.5194/acp-9-7551-2009.

Heaton, K. J., R. L. Sleighter, P. G. Hatcher, W. A. Hall IV, and M. V. Johnston (2009), Composition domains in monoterpene secondary organic aerosol, *Environ. Sci. Technol.*, *43*(20), 7797–7802, doi:10.1021/es901214p.

Jimenez, J. L., et al. (2009), Evolution of organic aerosols in the atmosphere, *Science*, *326*(5959), 1525–1529, doi:10.1126/science.1180353.

Joback, K. G., and R. C. Reid (1987), Estimation of pure-component properties from group-contributions, *Chem. Eng. Commun.*, *57*(1–6), 233–243, doi:10.1080/00986448708960487.

King, S. M., T. Rosenoern, J. E. Shilling, Q. Chen, and S. T. Martin (2007), Cloud condensation nucleus activity of secondary organic aerosol particles mixed with sulfate, *Geophys. Res. Lett.*, *34*, L24806, doi:10.1029/2007GL030390.

King, S. M., T. Rosenoern, J. E. Shilling, Q. Chen, and S. T. Martin (2009), Increased cloud activation potential of secondary organic aerosol for atmospheric mass loadings, *Atmos. Chem. Phys.*, *9*(9), 2959–2971, doi:10.5194/acp-9-2959-2009.

King, S. M., T. Rosenoern, J. E. Shilling, Q. Chen, Z. Wang, G. Biskos, K. A. McKinney, U. Pöschl, and S. T. Martin (2010), Cloud droplet activation of mixed organic-sulfate particles produced by the photooxidation of isoprene, *Atmos. Chem. Phys.*, *10*(8), 3953–3964, doi:10.5194/acp-10-3953-2010.

Kroll, J. H., and J. H. Seinfeld (2008), Chemistry of secondary organic aerosol: Formation and evolution of low-volatility organics in the atmosphere, *Atmos. Environ.*, *42*(16), 3593–3624, doi:10.1016/j.atmosenv.2008.01.003.

Kroll, J. H., J. D. Smith, D. L. Che, S. H. Kessler, D. R. Worsnop, and K. R. Wilson (2009), Measurement of fragmentation and functionalization pathways in the heterogeneous oxidation of oxidized organic aerosol, *Phys. Chem. Chem. Phys.*, *11*(36), 8005–8014, doi:10.1039/b905289e.

Lambe, A. T., T. B. Onasch, P. Massoli, D. R. Croasdale, J. P. Wright, A. T. Ahern, L. R. Williams, D. R. Worsnop, W. H. Brune, and P. Davidovits (2011), Laboratory studies of the chemical composition and cloud condensation nuclei (CCN) activity of secondary organic aerosol (SOA) and oxidized primary organic aerosol (OPOA), *Atmos. Chem. Phys.*, *11*(17), 8913–8928, doi:10.5194/acp-11-8913-2011.

Liu, B. Y. H., and K. W. Lee (1975), An aerosol generator of high stability, *Am. Ind. Hyg. Assoc. J.*, *36*(12), 861–865, doi:10.1080/00028897585073357.

Massoli, P., et al. (2010), Relationship between aerosol oxidation level and hygroscopic properties of laboratory generated secondary organic aerosol (SOA) particles, *Geophys. Res. Lett.*, *37*, L24801, doi:10.1029/2010GL045258.

Matsunaga, A., and P. J. Ziemann (2009), Yields of β-hydroxynitrates and dihydroxynitrates in aerosol formed from OH radical-initiated reactions of linear alkenes in the presence of NO_x, *J. Phys. Chem. A*, *113*(3), 599–606, doi:10.1021/jp807764d.

Matsunaga, A., and P. J. Ziemann (2010), Yields of β-hydroxynitrates, dihydroxynitrates, and trihydroxynitrates formed from OH radical-initiated reactions of 2-methyl-1-alkenes, *Proc. Natl. Acad. Sci. U. S. A.*, *107*(15), 6664–6669, doi:10.1073/pnas.0910585107.

Matsunaga, A., K. S. Docherty, Y. B. Lim, and P. J. Ziemann (2009), Composition and yields of secondary organic aerosol formed from OH radical-initiated reactions of linear alkenes in the presence of NO_x: Modeling and measurements, *Atmos. Environ.*, *43*(6), 1349–1357, doi:10.1016/j.atmosenv.2008.12.004.

Moore, R. H., and A. Nenes (2009), Scanning flow CCN analysis—A method for fast measurements of CCN spectra, *Aerosol Sci. Technol.*, *43*(12), 1192–1207, doi:10.1080/02786820903289780.

Odum, J. R., T. Hoffmann, F. Bowman, D. Collins, R. C. Flagan, and J. H. Seinfeld (1996), Gas/particle partitioning and secondary organic aerosol yields, *Environ. Sci. Technol.*, *30*(8), 2580–2585, doi:10.1021/es950943+.

Pankow, J. F. (1994), An absorption model of gas/particle partitioning of organic compounds in the atmosphere, *Atmos. Environ.*, *28*(2), 185–188, doi:10.1016/1352-2310(94)90093-0.

Petters, M. D., and S. M. Kreidenweis (2007), A single parameter representation of hygroscopic growth and cloud condensation nucleus activity, *Atmos. Chem. Phys.*, *7*(8), 1961–1971, doi:10.5194/acp-7-1961-2007.

Petters, M. D., A. J. Prenni, S. M. Kreidenweis, and P. J. DeMott (2007), On measuring the critical diameter of cloud condensation nuclei using mobility selected aerosol, *Aerosol Sci. Technol.*, *41*(10), 907–913, doi:10.1080/02786820701557214.

Petters, M. D., S. M. Kreidenweis, A. J. Prenni, R. C. Sullivan, C. M. Carrico, K. A. Koehler, and P. J. Ziemann (2009a), Role of molecular size in cloud droplet activation, *Geophys. Res. Lett.*, *36*, L22801, doi:10.1029/2009GL040131.

Petters, M. D., C. M. Carrico, S. M. Kreidenweis, A. J. Prenni, P. J. DeMott, J. L. Collett Jr., and H. Moosmüller (2009b), Cloud condensation nucleation activity of biomass burning aerosol, *J. Geophys. Res.*, *114*, D22205, doi:10.1029/2009JD012353.

Poulain, L., Z. Wu, M. D. Petters, H. Wex, E. Hallbauer, B. Wehner, A. Massling, S. M. Kreidenweis, and F. Stratmann (2010), Towards closing the gap between hygroscopic growth and CCN activation for secondary organic aerosols–Part 3: Influence of the chemical composition on the hygroscopic properties and volatile fractions of aerosols, *Atmos. Chem. Phys.*, *10*(8), 3775–3785, doi:10.5194/acp-10-3775-2010.

Prenni, A. J., M. D. Petters, S. M. Kreidenweis, P. J. DeMott, and P. J. Ziemann (2007), Cloud droplet activation of secondary organic aerosol, *J. Geophys. Res.*, *112*, D10223, doi:10.1029/2006JD007963.

Roberts, G. C., and A. Nenes (2005), A continuous-flow streamwise thermal-gradient CCN chamber for atmospheric measurements, *Aerosol Sci. Technol.*, *39*(3), 206–221, doi:10.1080/027868290913988.

Robinson, A. L., N. M. Donahue, M. K. Shrivastava, E. A. Weitkamp, A. M. Sage, A. P. Grieshop, T. E. Lane, J. R. Pierce, and S. N. Pandis (2007), Rethinking organic aerosols: Semivolatile emissions and photochemical aging, *Science*, *315*(5816), 1259–1262, doi:10.1126/science.1133061.

Rose, D., S. S. Gunthe, E. Mikhailov, G. P. Frank, U. Dusek, M. O. Andreae, and U. Pöschl (2008), Calibration and measurement uncertainties of a continuous-flow cloud condensation nuclei counter (DMT-CCNC): CCN activation of ammonium sulfate and sodium chloride aerosol particles in theory and experiment, *Atmos. Chem. Phys.*, *8*(5), 1153–1179, doi:10.5194/acp-8-1153-2008.

Shantz, N. C., W. R. Leaitch, L. Phinney, M. Mozurkewich, and D. Toom-Sauntry (2008), The effect of organic compounds on the growth rate of cloud droplets in marine and forest settings, *Atmos. Chem. Phys.*, *8*(19), 5869–5887, doi:10.5194/acp-8-5869-2008.

Shinozuka, Y., et al. (2009), Aerosol optical properties relevant to regional remote sensing of CCN activity and links to their organic mass fraction: Airborne observations over Central Mexico and the US West Coast during MILAGRO/INTEX-B, *Atmos. Chem. Phys.*, *9*(18), 6727–6742, doi:10.5194/acp-9-6727-2009.

Suda, S. R. (2011), Hygroscopicity frequency distributions of secondary organic aerosols, MS thesis, 152 pp., N. C. State Univ., Raleigh.

Sullivan, A. P., and R. J. Weber (2006), Chemical characterization of the ambient organic aerosol soluble in water: 1. Isolation of hydrophobic and hydrophilic fractions with a XAD-8 resin, *J. Geophys. Res.*, *111*, D05314, doi:10.1029/2005JD006485.

Sullivan, R. C., M. J. K. Moore, M. D. Petters, S. M. Kreidenweis, G. C. Roberts, and K. A. Prather (2009), Effect of chemical mixing state on the hygroscopicity and cloud nucleation properties of calcium mineral dust particles, *Atmos. Chem. Phys.*, *9*(10), 3303–3316, doi:10.5194/acp-9-3303-2009.

Taylor, W. D., T. D. Allston, M. J. Moscato, G. B. Fazekas, R. Kozlowski, and G. A. Takacs (1980), Atmospheric photodissociation lifetimes for nitromethane, methyl nitrite, and methyl nitrate, *Int. J. Chem. Kinet.*, *12*(4), 231–240, doi:10.1002/kin.550120404.

Tobias, H. J., and P. J. Ziemann (2001), Kinetics of the gas-phase reactions of alcohols, aldehydes, carboxylic acids, and water with the C13 stabilized Criegee intermediate formed from ozonolysis of 1-tetradecene, *J. Phys. Chem. A*, *105*(25), 6129–6135, doi:10.1021/jp004631r.

VanReken, T. M., N. L. Ng, R. C. Flagan, and J. H. Seinfeld (2005), Cloud condensation nucleus activation properties of biogenic secondary organic aerosol, *J. Geophys. Res.*, *110*, D07206, doi:10.1029/2004JD005465.

Wang, J., Y.-N. Lee, P. H. Daum, J. Jayne, and M. L. Alexander (2008), Effects of aerosol organics on cloud condensation nucleus (CCN) concentration and first indirect aerosol effect, *Atmos. Chem. Phys.*, *8*(21), 6325–6339, doi:10.5194/acp-8-6325-2008.

Wexler, A. S., and S. L. Clegg (2002), Atmospheric aerosol models for systems including the ions H^+, NH_4^+, Na^+, SO_4^{2-}, NO_3^-, Cl^-, Br^-, and H_2O, *J. Geophys. Res.*, *107*(D14), 4207, doi:10.1029/2001JD000451.

Yu, J., D. R. Cocker, R. J. Griffin, R. C. Flagan, and J. H. Seinfeld (1999), Gas-phase ozone oxidation of monoterpenes: Gaseous and particulate products, *J. Atmos. Chem.*, *34*(2), 207–258, doi:10.1023/A:1006254930583.

Ziemann, P. J. (2005), Aerosol products, mechanisms, and kinetics of heterogeneous reactions of ozone with oleic acid in pure and mixed particles, *Faraday Discuss.*, *130*, 469–490, doi:10.1039/b417502f.

S. M. Kreidenweis and R. C. Sullivan, Department of Atmospheric Science, Colorado State University, Fort Collins, CO 80523-1371, USA.

A. Matsunaga and P. J. Ziemann, Air Pollution Research Center, University of California, Riverside, CA 92521-0001, USA.

M. D. Petters and S. R. Suda, Department of Marine Earth and Atmospheric Sciences, North Carolina State University, Campus Box 8208, Raleigh, NC 27695-8208, USA. (markus_petters@ncsu.edu)